Mott insulators in strong electric fields

Subir Sachdev,* K. Sengupta,† and S. M. Girvin‡
Department of Physics, Yale University, P.O. Box 208120, New Haven, Connecticut 06520-8120
(Received 18 May 2002; published 30 August 2002)

Recent experiments on ultracold atomic gases in an optical lattice potential have produced a Mott insulating state of ^{87}Rb atoms. This state is stable to a small applied potential gradient (an ''electric'' field), but a resonant response was observed when the potential energy drop per lattice spacing (E), was close to the repulsive interaction energy (U) between two atoms in the same lattice potential well. We identify all states which are resonantly coupled to the Mott insulator for $E \approx U$ via an infinitesimal tunneling amplitude between neighboring potential wells. The strong correlation between these states is described by an effective Hamiltonian for the resonant subspace. This Hamiltonian exhibits quantum phase transitions associated with an Ising density wave order and with the appearance of superfluidity in the directions transverse to the electric field. We suggest that the observed resonant response is related to these transitions and propose experiments to directly detect the order parameters. The generalizations to electric fields applied in different directions and to a variety of lattices should allow study of numerous other correlated quantum phases.

DOI: 10.1103/PhysRevB.66.075128 PACS number(s): 71.10.Hf, 03.75.Fi, 67.90.+z, 32.80.Pj

I. INTRODUCTION

Recent experiments on ultracold trapped atomic gases have opened a new window onto the phases of quantum matter.[1,2] A gas of bosonic atoms has been reversibly tuned between superfluid and insulating ground states by varying the strength of a periodic potential produced by standing waves of laser light.[2] These experiments offer unprecedented control of the microscopic parameters and allow exploration of parameter regimes not previously available in analogous condensed matter systems.

This paper focuses on one such ''extreme'' parameter regime. Let w be the amplitude for an atom to tunnel between neighboring minima of the standing laser wave and U be the repulsive interaction energy between two atoms in the same potential well. When w is smaller than a value of order U, the ground state is a Mott insulator for certain values of the atomic density or chemical potential. In this state, the average number of atoms in each potential well must be an integer n_0 (see Fig. 1). Now consider ''tilting'' this Mott insulator[2]—i.e., placing it under an external potential which decreases linearly along a particular direction in space. Conceptually, it is useful to imagine that the atoms carry a fictitious ''charge,'' and then this potential gradient corresponds to applying a uniform ''electric'' field E (in practice this field is applied by changing the position of the center of the atomic trap[2]). We measure E in units of energy, defining E to be the maximal drop in potential energy of an atom moving between nearest-neighbor minima of the periodic potential [the potential energy drop depends upon the choice of the nearest neighbor, and we choose the direction(s) along which the drop is the largest to define E]. In almost all Mott insulators consisting of electrons or Cooper pairs, all reasonable electric fields that can be achieved in the laboratory are small enough so that the relation $E \ll w, U$ is well satisfied. Remarkably, in the new atomic systems significantly larger ''electric'' fields are easily achievable: This paper shall discuss the regime $E \sim U$ which has been explored in the recent experiments of Greiner *et al.*[2] More precisely, we shall discuss the regime

$$|U-E|, w \ll E, U, \tag{1.1}$$

while allowing the ratio $(U-E)/w$ to be arbitrary.

We mention, in passing, another experimental system which has been studied under conditions analogous to Eq. (1.1). Electron transport has been investigated in arrays of GaAs quantum dots,[3] when the voltage drop between neighboring quantum dots (the analog of E) is at or above the charging energy required to make the transition (the analog of U). However, in these systems the excess electron energy can be dissipated away to the underlying lattice, and so it

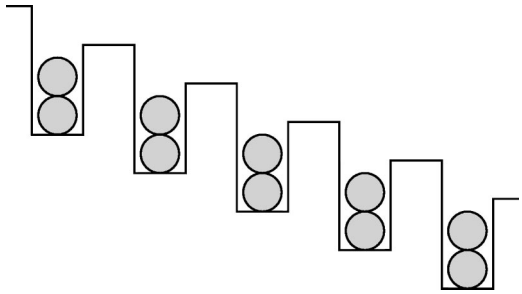

FIG. 1. Schematic representation of the Mott insulator and of various states coupled to it. Shown above is the Mott insulator with $n_0=2$. Each well represents a local minimum of the optical lattice potential—these we number 1–5 from the left. The potential gradient leads to a uniform decrease in the on-site energy of atom as we move to the right. The gray circles are the b_i bosons of Eq. (1.2). The vertical direction represents increasing energy: the repulsive interaction energy between the atoms is realized by placing atoms vertically within each well, so that each atom displaces the remaining atoms upwards along the energy axis. We have chosen the diameter of the atoms to equal the potential energy drop between neighboring wells—this corresponds to the condition $U=E$. Consequently, *a resonant transition is one in which the top atom in a well moves horizontally to the top of a nearest-neighbor well*; motions either upwards or downwards are nonresonant.

appears that the threshold behavior can be described by dissipative classical models.[4] In contrast, for the atomic systems of interest in the present paper, there is essentially no dissipation over the time scales of interest, and a fully quantum treatment must be undertaken.

It is useful to explicitly state our model Hamiltonian for the Mott insulator for our subsequent discussion. We will consider only Mott insulators of bosons, although the extension to fermionic Mott insulators is possible.[5] We label the minima of the periodic potential by lattice sites i and assume that all bosons occupy a single band of ''tight-binding'' orbitals centered on these sites. Let $b_i^\dagger$ be the creation operator for a boson on site i. We will study the boson Hubbard model[6–8]

$$\mathcal{H} = -w\sum_{\langle ij\rangle}\,(b_i^\dagger b_j + b_j^\dagger b_i) + \frac{U}{2}\sum_i\, n_i(n_i-1) - E\sum_i\,\mathbf{e}\cdot\mathbf{r}_i n_i\,, \tag{1.2}$$

where $\langle ij\rangle$ represents pairs of nearest-neighbor sites,

$$n_i \equiv b_i^\dagger b_i\,, \tag{1.3}$$

$\mathbf{r}_i$ are the spatial coordinates of the lattice sites (the lattice spacing is unity), and $\mathbf{e}$ is a vector in the direction of the applied electric field ($\mathbf{e}$ is not necessarily a unit vector—its length is determined by the strength of the electric field, the lattice structure, and our definition of E above). We will mainly consider simple cubic lattices, with the $\mathbf{e}$ oriented along one of the lattice directions and of unit length. Not shown in Eq. (1.2) is an implied chemical potential term which is chosen so that the average density of atoms per site is n_0. We will restrict our attention to the case where n_0 is of order unity.

Some simple key points can be made by first considering the noninteracting case $U=0$, and also by simplifying to one spatial dimension.[9] For this special case, we can write $\mathcal{H}$ as

$$\mathcal{H}_0 = -\sum_l\,(wb_l^\dagger b_{l+1} + wb_{l+1}^\dagger b_l + Elb_l^\dagger b_l), \tag{1.4}$$

where l is an integer labeling the lattice sites. The exact single-particle eigenstates of $\mathcal{H}_0$ can be easily obtained: the eigenenergies form a Wannier-Stark ladder, and the most important property of the wave functions is that they are all *localized*. Specifically, the eigenstates can be labeled by an integer m which runs from $-\infty$ to ∞, the exact eigenenergies are

$$\epsilon_m = Em, \tag{1.5}$$

and the corresponding exact and normalized wave functions can be expressed in terms of Bessel functions:

$$\psi_m(l) = J_{l-m}(2w/E); \tag{1.6}$$

for a derivation see, e.g., Ref. 10 (their analysis is in a different gauge). The mth state is localized near the site $l=m$, and for large $|l-m|$ its wave function decays as

$$|\psi_m(l)| \sim \exp\left[-|l-m|\ln\left(\frac{|l-m|E}{ew}\right)\right]; \tag{1.7}$$

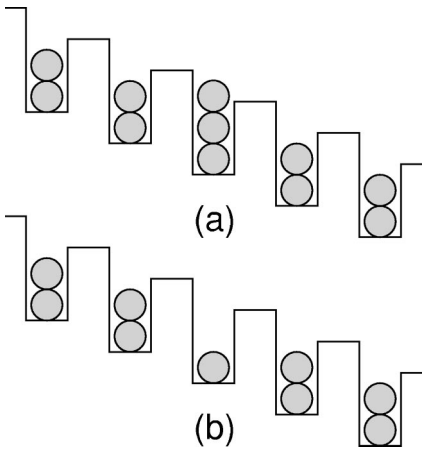

FIG. 2. Schematic representation of the Mott insulator and of various states coupled to it. Notation as in Fig. 1. (a) A quasiparticle on site 3; the motion of this quasiparticle is described by the localized wave functions (1.6) but with w replaced by $3w$. (b) A quasihole on site 3; the motion of this quasihole is also described by the localized wave functions (1.6) but with w replaced by $2w$.

the decay is faster than exponential and is extremely rapid under the conditions (1.1). The reader should resist the temptation to imagine that a particle placed initially at the site l will eventually be accelerated by the applied electric field out to infinity. Instead, the particle remains localized near its initial site and undergoes *Bloch oscillations* with period h/E; indeed, as is clear from the simple form of Eq. (1.5), its wave function is exactly equal to its initial wave function at regular time intervals of h/E. The particle can escape to infinity only with a process of Zener tunneling to higher bands not included in the single-band tight-binding models in Eqs. (1.4) and (1.2); the probability of such tunneling is negligibly small in the experiments of interest here and so will be ignored in our analysis.

We now return our discussion to the full Hubbard model Eq. (1.2). As was the case in (1.5), the spectrum of this Hamiltonian is unbounded from below for $E\neq 0$, and so it does not make sense to ask for its ''ground state'' for any density of particles. Rather, guided by the experimental situation of Ref. 2, we are interested in states which are accessible from the translationally invariant Mott state (with an average of n_0 particles on every site) over the experimentally relevant time scales. The experiment[2] begins at $E=0$ with a Mott insulator with n_0 particles per site, rapidly ramps up E to a value of order U, and detects the change in the state. For $w \ll U$ and for most values of E, the experiments displayed little detectable change in the state of the system. We can initially understand this by a simple extension of the argument presented above for the noninteracting model $\mathcal{H}_0$. Consider a ''quasiparticle'' state of the Mott insulator, created by adding a single additional particle on one site, as shown in Fig. 2(a). To leading order in w/U, the motion of this quasiparticle along the direction $\mathbf{e}$ is described by an effective Hamiltonian which is identical in form to $\mathcal{H}_0$, but with the hopping matrix element w replaced $w(n_0+1)$. So any such quasiparticle states created above the Mott insulator will remain localized and will not have the chance to extend across

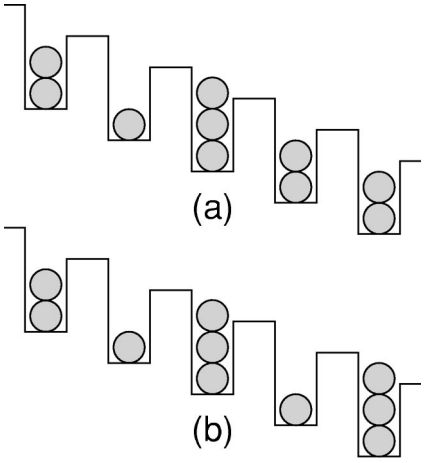

FIG. 3. Schematic representation of the Mott insulator and of various states coupled to it. Notation as in Fig. 1. (a) A dipole on sites 2 and 3; this state is resonantly coupled by an infinitesimal w to the Mott insulator in (a) when $E=U$. (b) Two dipoles between sites 2 and 3 and between 4 and 5; this state is connected via multiple resonant transitions to the Mott insulator for $E=U$.

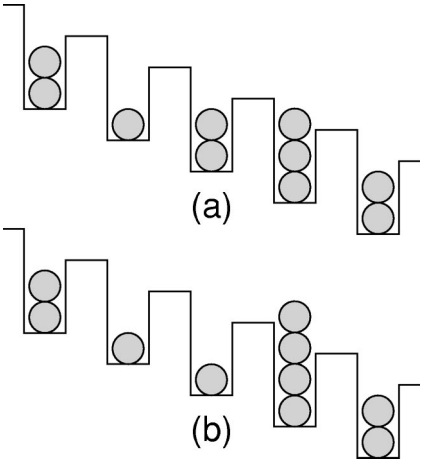

FIG. 4. Schematic representation of the Mott insulator and various states coupled to it. Notation as in Fig. 1. Two states which are not part of the resonant manifold. (a) An attempt to create dipoles between sites 2 and 3 and also between sites 3 and 4; the result is a single dipole of length 2 which has energy $U-2E$ relative to the Mott insulator, and so this long dipole is *not* part of the resonant family of states. (b) A state with energy $3(U-E)$ relative to the Mott insulator; this state is not part of the resonant family because its largest effective matrix element to any state in the resonant family is of order w^2/U [for $U=E$; see Eq. (1.8)]. In contrast, all states within the resonant family are connected to at least one other state also in the family by a matrix element of order w.

the system to create large changes in the initial state. A similar localization argument applies to the quasihole state shown in Fig 2(b): it experiences an electric force in the opposite direction, the effective hopping matrix element is wn_0, and all quasihole states are also all localized in the direction **e**. Indeed, it is not difficult to see that the same localization argument applies to all deformations of the Mott insulator which carry a net charge.

The important exceptions to the above argument for the stability of the Mott state are deformations which carry no net charge. It is the primary purpose of this paper to describe the collective properties of such neutral states. They will be shown to yield a resonantly strong effect on the Mott state when $E\sim U$, which has been dramatically observed in the experiments of Greiner *et al.*[2] Indeed, Greiner *et al.* have already identified an important neutral deformation of the Mott state—it is the *dipole* state consisting of a quasiparticle-quasihole pair on nearest-neighbor sites, as shown in Fig. 3(a). A key consequence of our discussion above is that, for $w\ll E$ (a condition we assume throughout), we can safely neglect the independent motion of the quasiparticle and of the quasihole along the direction of **e**. Only their paired motion as dipoles will be important along **e**, although they can move independently along directions orthogonal to **e**.

For $w=0$, the dipole state in Fig. 3(a) differs in energy from the Mott state by $U-E$. So these states become degenerate at $U=E$, and an infinitesimal w leads to a *resonant* coupling between them. However, there are a large number of other states which are resonantly coupled to one of more of these states, and they also have to be treated on an equal footing. Indeed, it is sufficient for an given state to be resonantly coupled to any one other state in the manifold of resonant states for it to be an equal member of the resonant family—it is *not* necessary to have a direct resonant coupling to the parent Mott insulator. The reader should already notice that multiple dipole deformations of the Mott insulator [like the state in Fig. 3(b)] are part of the resonant family. In dimensions greater than one, these dipole states are only a small fraction of the set of resonant states, as we will show below. We are now in a position to succinctly state the purpose of this paper: *identify the complete set of states resonantly coupled to the Mott state under the conditions (1.1), obtain the effective Hamiltonian within the subspace of these states, and determine its spectrum and correlations.* The results will allow us to address the strong response of the Mott insulator to an electric field $E\sim U$ observed by Greiner *et al.*[2] and lead to some definite predictions which can be tested in future experiments.

The first step in our program is a complete description of the set of resonant states. We will do this first for one dimension in the Sec. I A and for all higher dimensions in Sec. I B. The effective Hamiltonian in the resonant subspace will be shown to contain strong correlations among its degrees of freedom, but we will demonstrate that these can be satisfactorily treated by available analytic and numerical methods in many-body theory. Before embarking on a detailed description of our computation, the reader may find it useful to examine Figs. 3 and 4 for an understanding of the origin of the strong correlations in the one-dimensional case. Figure 3 contains only dipole states: notice that while resonant dipole states can be created separately on nearest-neighbor links, it is not possible to create two dipoles simultaneously on such links [as in Fig. 4(a)] without violating the resonant conditions. This implies an infinite repulsive interaction between nearest-neighbor dipoles in the effective Hamiltonian. Two (or more) dipoles can be safely created when they are farther apart, as shown in Fig. 3(b). Thus the dipole resonances are

not independent of each other, and the wave function contains nontrivial ''entanglements'' between them.

A. One dimension

It is not difficult to see that, in one spatial dimension, the set of all nearest-neighbor dipole states constitutes the entire family of states resonantly coupled to the Mott insulator in Fig. 1 for $U=E$ and an infinitesimal w. The only subtlety concerns states like those in Fig. 4(b), which are not made up of nearest-neighbor dipoles. For $w=0$, this state has energy $3(U-E)$ relative to that in Fig. 1. However, reaching the state in Fig. 4(b) from any state in the resonant family requires a detour through a nonresonant state. A simple second-order perturbation theory calculation shows that the closest state from the resonant family connected to Fig. 4(b) is a state with dipoles between sites 3 and 4 and that the effective matrix element between them is

$$\frac{w^2 n_0\sqrt{n_0(n_0+1)}}{2}\left(\frac{1}{U}+\frac{1}{2U-E}\right); \tag{1.8}$$

this is negligibly small, under the conditions (1.1), compared to the nonzero matrix elements $(=w)$ between states within the resonant family. Hence we can safely neglect the state in Fig. 4(b). More completely, the argument is that after we diagonalize the Hamiltonian within the resonant family, states coupled to that in Fig. 4(b) will differ from it by an energy of order w; the coupling in Eq. (1.8) will then be too weak to induce a resonance.

It is convenient now to introduce bosonic dipole creation operators $d_l^\dagger$ to allow us to specify the resonant subspace and its effective Hamiltonian. Let $|Mn_0\rangle$ be the Mott insulator with n_0 particles on every site (the state in Fig. 1 is $|M2\rangle$). We identify this state with the dipole vacuum $|0\rangle$. Then the single dipole state is

$$d_l^\dagger|0\rangle \equiv \frac{1}{\sqrt{n_0(n_0+1)}} b_l b_{l+1}^\dagger |Mn_0\rangle. \tag{1.9}$$

Notice that we have placed the dipole operator on the left edge of the dipole which actually resides on links between the lattice sites. Clearly, we cannot create more than one dipole resonantly on the same link: hence the dipoles satisfy an on-site hard core constraint

$$d_l^\dagger d_l \leqslant 1. \tag{1.10}$$

Moreover, we cannot create two dipoles simultaneously on nearest-neighbor links—this leads to a nonresonant state like that in Fig. 4(a); such states are prohibited by a hard-core repulsion between nearest-neighbor sites:

$$d_l^\dagger d_l d_{l+1}^\dagger d_{l+1} = 0. \tag{1.11}$$

The resonant family of states can now be completely specified as the set of all states of the boson d_l which satisfy Eqs. (1.10) and (1.11). A typical state is sketched in Fig. 5(a). Notice that the dipole vacuum $|Mn_0\rangle$ is one of the allowed states.

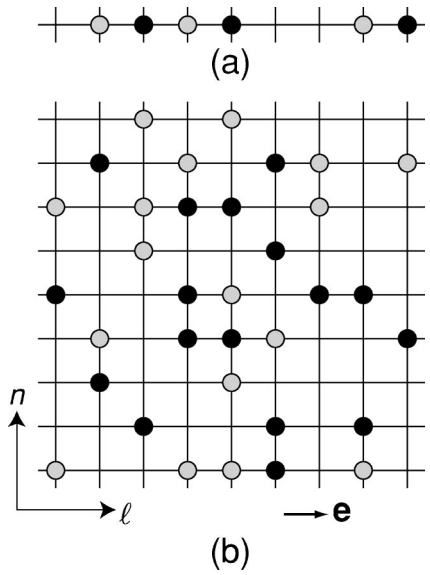

FIG. 5. Typical states in the resonant subspace for (a) $D=1$ and (b) $D=2$. Black circles represent sites with quasiparticles (these sites have $n_i=n_0+1$ [see Eq. (1.3)] and gray circles represent quasiholes (these sites have $n_i=n_0-1$), while the remaining sites have $n_i=n_0$. Note that Q_l in Eq. (1.17) is zero for each column; i.e., the total number of quasiparticles in every column equals the total number of quasiholes in the column to its immediate left. Only in $D=1$ does this constraint imply that all states contain only nearest-neighbor dipoles.

It is now a simple matter to write down the effective Hamiltonian $\mathcal{H}_d$ for the d_l. It costs energy $U-E$ to create each dipole, and each dipole can be created or annihilated with an amplitude of order w (this corresponds to the horizontal motion of particles in Figs. 1–4). So we have

$$\mathcal{H}_d = -w\sqrt{n_0(n_0+1)}\sum_l (d_l+d_l^\dagger)+(U-E)\sum_l d_l^\dagger d_l. \tag{1.12}$$

The Hamiltonian (1.12), along with the constraints (1.10) and (1.11), constitute one of the correlated many-body problems we shall analyze in this paper. The eigenstates of $\mathcal{H}_d$ are characterized by n_0 and the single dimensionless number

$$\lambda \equiv \frac{U-E}{w}, \tag{1.13}$$

and a description of their properties as λ ranges over all real values is in Sec. II. [Strictly speaking, the eigenstates of $\mathcal{H}_d$ depend only $\lambda/\sqrt{n_0(n_0+1)}$, but λ and n_0 do not combine into a single constant in higher dimensions.]

It is interesting to note that there is no explicit hopping term for the d_l bosons in $\mathcal{H}_d$: it appears that the bosons are only allowed to be created from, and to disappear into, the vacuum by the first term in Eq. (1.12). However, this is misleading: as we will see in Sec. II, the combination of the terms in Eq. (1.12) and the constraint (1.11) does generate a local hopping term for the d_l bosons [see Eq. (2.1)]. Additional dipole hopping terms also arise from virtual processes of order w^2/U in the underlying Hubbard model $\mathcal{H}$; how-

ever, these are negligibly small compared to those just mentioned and do not need to be included in $\mathcal{H}_d$.

We close this subsection by noting that the Hamiltonian $\mathcal{H}_d$ in Eq. (1.12) and the constraints (1.10) and (1.11) can also be written in the form of a quantum spin chain. We identify the dipole present-absent configuration on a site l as a pseudospin σ_l^z up/down ($\sigma^{x,y,z}$ are the Pauli matrices). Then $\sigma_l^z = 2d_l^\dagger d_l - 1$ and

$$\mathcal{H}_d = \sum_l \left[-w\sqrt{n_0(n_0+1)}\,\sigma_l^x + (U-E)(\sigma_l^z+1)/2 + J(\sigma_l^z+1)(\sigma_{l+1}^z+1)\right]. \tag{1.14}$$

The constraint (1.11) is implemented by taking the $J\to\infty$ limit of the last term. The spin chain model so obtained is an $S=1/2$ Ising spin chain in *both* transverse and longitudinal fields. This is known not to be integrable for finite J, but it does appear that the problem simplifies in the $J\to\infty$ limit we consider here.

B. Higher dimensions

We consider here only hypercubic lattices in D spatial dimensions, with **e** oriented along one of the principal cubic axes and a lattice spacing in length [e.g., $D=3$ and **e** $=(1,0,0)$]. Other lattices and other directions of **e** also allow for interesting correlated phases and these will be mentioned in Sec. IV.

Extension of our reasoning above quickly shows that the dipole states now constitute only a negligibly small fraction of the set of states in the resonant family. Once a dipole has been created on a pair of sites separated by the vector **e**, its quasiparticle and quasihole constituents can move freely and resonantly, with matrix elements of order w, in the $(D-1)$ directions orthogonal to **e**. Allowing this process to occur repeatedly (while maintaining some constraints discussed below), we can build up the set of all resonantly coupled states. A typical resonant state in $D=2$ is shown in Fig. 5(b). As in Sec. I A, it is useful to give an operator definition of the resonant family. To allow us to distinguish between the directions parallel and orthogonal to **e**, we replace the D-dimensional site label i by the composite label (l,n), where l is an integer measuring the coordinate along **e** (as in the one-dimensional case), while n is a label for sites along the $(D-1)$ transverse directions. Rather than using dipole operators, we now want to work with bosonic quasiparticle ($p_{l,n}^\dagger$) and quasihole ($h_{l,n}^\dagger$) operators, which create states like those in Figs. 2(a) and 2(b), respectively. More precisely, we now identify $|Mn_0\rangle$ with quasiparticle and quasihole vacuum $|0\rangle$, and so

$$p_{l,n}^\dagger|0\rangle \equiv \frac{1}{\sqrt{n_0+1}} b_{l,n}^\dagger |Mn_0\rangle,$$

$$h_{l,n}^\dagger|0\rangle \equiv \frac{1}{\sqrt{n_0}} b_{l,n}|Mn_0\rangle. \tag{1.15}$$

The set of resonant states can now be specified by a few simple constraints on these operators, which are the analogs of Eqs. (1.10) and (1.11). First, there are the obvious on-site hard-core constraints that no site can have more than one particle or hole:

$$p_{l,n}^\dagger p_{l,n} \leqslant 1,$$

$$h_{l,n}^\dagger h_{l,n} \leqslant 1,$$

$$p_{l,n}^\dagger p_{l,n} h_{l,n}^\dagger h_{l,n} = 0. \tag{1.16}$$

Additionally, because of the manner in which these quasiparticles and quasiholes appear from the Mott state, the total number of quasiparticles in the $(D-1)$-dimensional layer with coordinate $l+1$ must equal the total number of quasiholes in layer l:

$$Q_l \equiv \sum_n \left(p_{l+1,n}^\dagger p_{l+1,n} - h_{l,n}^\dagger h_{l,n}\right) = 0. \tag{1.17}$$

While the quasiparticles and quasiholes are allowed to move freely within each $(D-1)$-dimensional layer, they cannot move resonantly out of any layer on their own; this is, of course, related to the localization of the Wannier-Stark ladder states discussed earlier in this section.

Continuing the analogy with Sec. I A, we can now easily write down the effective Hamiltonian $\mathcal{H}_{ph}$ for the quasiparticles and quasiholes which acts on the set of states defined by Eqs. (1.16) and (1.17). The terms in the first two lines are the same as those already present in Eq. (1.12), but expressed now in terms of the quasiparticle-hole operators, while the last line is associated with motion along the transverse $D-1$ directions:

$$\mathcal{H}_{ph} = -w\sqrt{n_0(n_0+1)} \sum_{l,n} \left(p_{l+1,n} h_{l,n} + p_{l+1,n}^\dagger h_{l,n}^\dagger\right) + \frac{(U-E)}{2} \sum_{l,n} \left(p_{l,n}^\dagger p_{l,n} + h_{l,n}^\dagger h_{l,n}\right) - w \sum_{l,\langle nm\rangle} \left(n_0 h_{l,n}^\dagger h_{l,m} + (n_0+1) p_{l,n}^\dagger p_{l,m} + \text{H.c.}\right). \tag{1.18}$$

Here $\langle nm\rangle$ represents a nearest-neighbor pair of sites within a single $(D-1)$-dimensional layer orthogonal to **e**. Notice that all the Q_l in Eq. (1.17) commute with $\mathcal{H}_{ph}$, as is required for the consistency of our approach. As was the case in one dimension, the properties of $\mathcal{H}_{ph}$ are determined by the single dimensionless constant λ in Eq. (1.13); these will be described in Sec. III.

It is worth reiterating explicitly here that upon specialization to the case of $D=1$ (when the indices n,m only have a single allowed value and the set $\langle nm\rangle$ is empty), the Hamiltonian $\mathcal{H}_{ph}$ above is exactly equivalent to the one-dimensional dipole model H_d in Eq. (1.12).

We note in passing that in a manner similar to $\mathcal{H}_d$, $\mathcal{H}_{ph}$ in Eq. (1.18) can also be written as a $S=1$ spin model, with the empty-qausiparticle-quasihole states on a site corresponding to spin states with $S_z = 0, 1, -1$.

The outline of the remainder of the paper is as follows. The properties the $D=1$ model $\mathcal{H}_d$ will be described in Sec. II, while the $D>1$ model $\mathcal{H}_{ph}$ will be considered in Sec. III. We discuss extensions of our results to other lattices and field

directions in Sec. IV. Implications of our results for experiments appear in Sec. V. The Appendixes contain some technical discussion of the nature of the quantum phase transitions found in the body of the paper.

II. DIPOLE PHASES IN ONE DIMENSION

This section will describe the spectrum of the one-dimensional dipole Hamiltonian $\mathcal{H}_d$ in Eq. (1.12), subject to the constraints (1.10) and (1.11).

An essential point becomes clear simply by looking at the limiting cases $\lambda \to \infty$ and $\lambda \to -\infty$ [the coupling λ was defined in Eq. (1.13)]. For $\lambda \to \infty$ the ground state of $\mathcal{H}_d$ is the nondegenerate dipole vacuum $|0\rangle$. In contrast, for $\lambda \to -\infty$ the ground state is doubly degenerate, because there are two distinct states with maximal dipole number: $(\cdots d_1^\dagger d_3^\dagger d_5^\dagger \cdots)|0\rangle$ and $(\cdots d_2^\dagger d_4^\dagger d_6^\dagger \cdots)|0\rangle$. This immediately suggests the existence of an Ising quantum critical point at some intermediate value of λ, associated with an order parameter which is a density wave of dipoles of period two lattice spacings. We will shortly present numerical evidence which strongly supports this conclusion.

Further analytic evidence for an Ising quantum critical point can be obtained by examining the excitation spectra for the limiting λ regimes and noting their similarity to those on either side of the critical point in the quantum Ising chain.[11]

For $\lambda \to \infty$, the lowest excited states are the single dipoles: $|l\rangle = d_l^\dagger|0\rangle$; there are N such states (N is the number of sites), and at $\lambda = \infty$, they are all degenerate at energy $U-E$. The degeneracy is lifted at second order in a perturbation theory in $1/\lambda$: By a standard approach using canonical transformations, these corrections can be described by an effective Hamiltonian $\mathcal{H}_{d,\mathrm{eff}}$ that acts entirely within the subspace of single-dipole states. We find

$$\mathcal{H}_{d,\mathrm{eff}} = (U-E)\sum_l \left[|l\rangle\langle l| + \frac{n_0(n_0+1)}{\lambda^2} \times (|l\rangle\langle l| + |l\rangle\langle l+1| + |l+1\rangle\langle l|) \right]. \quad (2.1)$$

Notice that, quite remarkably, a local dipole hopping term has appeared, as we promised earlier at the end of Sec. I A. The constraints (1.10) and (1.11) played a crucial role in the derivation of Eq. (2.1). Upon considering perturbations to $|l\rangle$ from the first term in Eq. (1.12) it initially seems possible to obtain an effective matrix element between any two states $|l\rangle$ and $|l'\rangle$. However, this connection can generally happen via two possible intermediate states $|l\rangle \to d_l^\dagger d_{l'}^\dagger |0\rangle \to |l'\rangle$ and $|l\rangle \to |0\rangle \to |l'\rangle$, and the contributions of the two processes exactly cancel each other for most l, l'. Only when the constraints (1.10) and (1.11) block the first of these processes is a residual matrix element possible, and these are shown in Eq. (2.1). It is a simple matter to diagonalize $\mathcal{H}_{d,\mathrm{eff}}$ by going to momentum space, and we find a single band of dipole states. The lowest-energy dipole state has momentum π: The softening of this state upon reducing λ is then consistent with the appearance of density wave order of period 2. The higher excited states at large λ consist of multiparticle continua of this band of dipole states, just as in the Ising chain.[11]

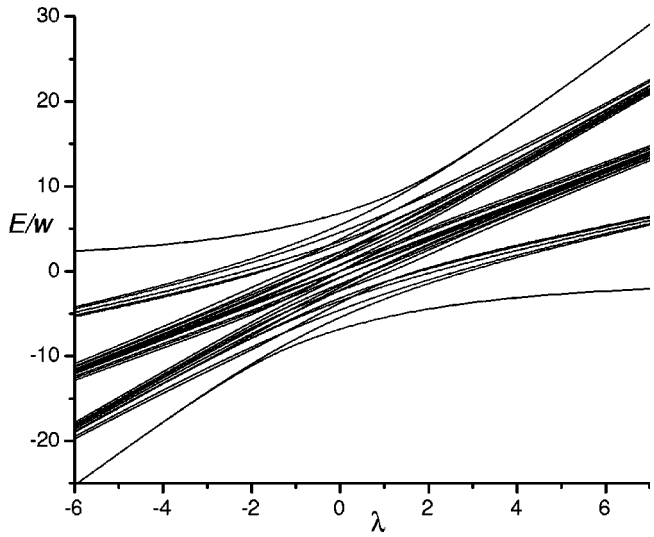

FIG. 6. All the eigenvalues of $\mathcal{H}_d$ for $N=8$ and $n_0=1$. Note that the ground state is non-degenerate for positive λ, and there are two low-lying levels with an exponentially small splitting for $\lambda < 0$ and $|\lambda|$ large.

A related analysis can be carried out for $\lambda \to -\infty$, and the results are very similar to those for the ordered state in the quantum Ising chain.[11] The lowest excited states are single bands of domain walls between the two filled dipole states, and above them are the corresponding multiparticle continua.

Exact diagonalization

We numerically determined the exact spectrum of $\mathcal{H}_d$ for lattice sizes up to $N=18$. As will be evident below, these sizes were adequate to reliably extract the limiting behavior of the $N \to \infty$ limit.

The complete spectrum of $\mathcal{H}_d$ is shown in Fig. 6 for $N=8$ and $n_0=1$. We used periodic boundary conditions on the dipole Hamiltonian in Eq. (1.12). Note that these do not correspond to periodic boundary conditions for the original model (1.2); indeed, for Eq. (1.2) the presence of the electric field implies that periodic boundary conditions are not physically meaningful. Nevertheless, it is useful to apply periodic boundary conditions to the translationally invariant effective model (1.12), merely as a mathematical tool for rapidly approaching the $N \to \infty$ limit. Note that Fig. 6 shows a unique ground state for $\lambda \to \infty$ and a twofold-degenerate state for $\lambda \to -\infty$. Above these lowest-energy states, there is a finite energy gap, and the excited states have clearly split into bands corresponding to the various ''particle'' continua; these ''particles'' are dipoles for $\lambda \to \infty$ and domain walls between the two ground states for $\lambda \to -\infty$, as we discussed in the perturbative analysis above.

We test for a quantum critical point at intermediate values of λ by plotting the energy gap, Δ, in Fig. 7. This gap is the spacing the between the lowest two of the eigenvalues plotted in Fig. 6 (for finite system sizes, these low-lying levels are always nondegenerate). It becomes exponentially small

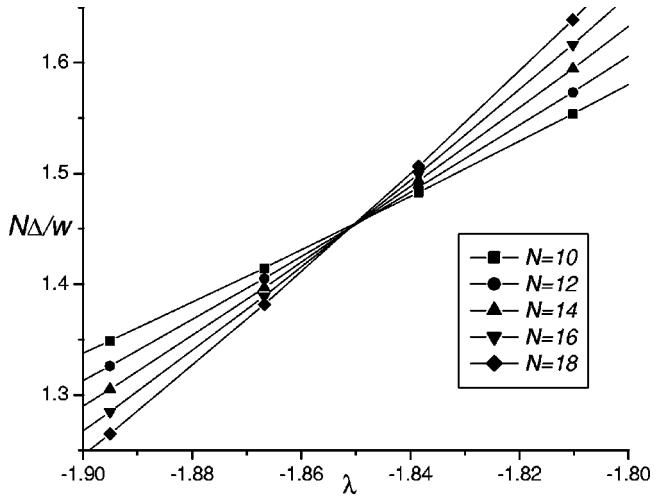

FIG. 7. The spacing between the lowest two eigenvalues of $\mathcal{H}_d$ $(=\Delta)$ as a function λ for various system sizes and $n_0=1$. We used periodic boundary conditions for $\mathcal{H}_d$.

in the system size as we approach the two degenerate ground states which are present for λ sufficiently negative. In the opposite limit, Δ approaches a finite nonzero value, which becomes $U-E$, for λ large and positive. If these two phases are separated by a quantum critical point, we expect the energy gap to scale as $\Delta \sim N^{-z}$ at the critical point $\lambda=\lambda_c$, where z is the dynamic critical exponent. The Ising critical point has $z=1$, and so Fig. 7 plots $N\Delta$ as a function of λ. We observe a clear crossing point at $\lambda_c \approx -1.850$ which we identify as the position of the Ising quantum phase transition. Note that the critical point is shifted away from the naive value $E=U$ $(\lambda=0)$ to $E>U$ because of quantum fluctuations associated with the hopping of the dipoles.

A second test of Ising criticality is provided by also rescaling the horizontal axis of Fig. 7 with N. General finite-size scaling arguments imply that the energy gap should obey the scaling form

$$\Delta = N^{-z}\phi(N^{1/\nu}(\lambda-\lambda_c)), \tag{2.2}$$

where ϕ is a universal scaling function and ν is the correlation length exponent. We test for Eq. (2.2) in Fig. 8 with the Ising exponent $\nu=1$ and again find excellent agreement.

A final and most sensitive test for Ising criticality is provided by a measurement of the anomalous dimension of the order parameter. The order parameter is the density of dipoles at momentum π, and so we computed its equal-time structure factor

$$S_\pi = \frac{1}{N}\left\langle \left(\sum_l (-1)^l d_l^\dagger d_l \right)^2 \right\rangle. \tag{2.3}$$

Standard scaling arguments imply that this should scale as $N^{2-z-\eta}$ at $\lambda=\lambda_c$, where η is the anomalous dimension of the order parameter. Using the Ising exponent $\eta=1/4$, we expect $S_\pi \sim N^{3/4}$. This is tested in Fig. 9. Note that there is an excellent crossing point at $\lambda_c \approx -1.853$. This position of the crossing point is completely consistent with the crossing point found in Fig. 7. Thus Fig. 9 provides strong evidence

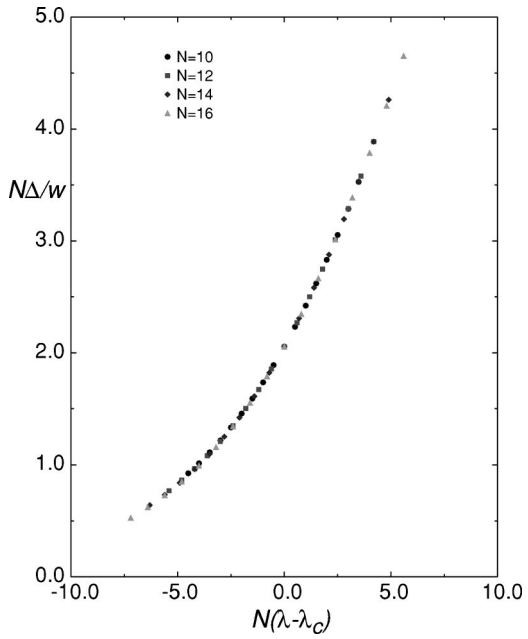

FIG. 8. Scaling plot of the energy gap to test for Eq. (2.2). We used $\lambda_c=-1.850$ and $n_0=1$.

for the expected Ising exponent $\eta=1/4$. We have also examined a plot which scales the horizontal axis in Fig. 9 as in Fig. 8: The data collapse is again excellent.

III. QUASIPARTICLE AND QUASIHOLE PHASES IN HIGHER DIMENSIONS

This section will discuss the properties of the $D>1$ dimensional model of the $p_{l,n}$ quasiparticles and $h_{l,n}$ quasiholes described the Hamiltonian $\mathcal{H}_{ph}$ in Eq. (1.18), subject to the constraints (1.16) and (1.17).

As in Sec. II, it is instructive to first look at the two distinct limiting values of λ. The nature of the ground states is very similar to those in $D=1$ for these ranges of λ. For $\lambda \to \infty$, we have a unique ground state which contains only small perturbations from the quasiparticle and quasihole

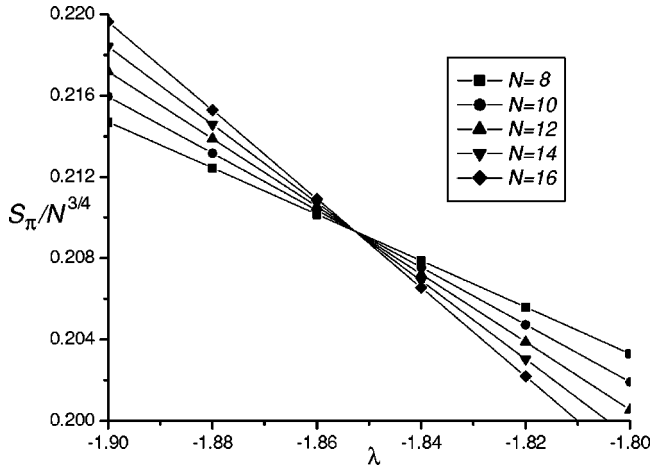

FIG. 9. Scaling plot of numerical results for the order parameter structure factor S_π defined in Eq. (2.3). We used $n_0=1$.

vacuum $|0\rangle$. For $\lambda \to -\infty$, it is clear that we want to maximize the total number of quasiparticles and quasiholes in the ground state, subject to the constraints (1.16) and (1.17). There are a very large number of ways of doing this, but by considering perturbative corrections to the ground-state energy in powers of $1/|\lambda|$, it is not difficult to see that it pays to choose one of two regular arrangements, in which the occupation numbers are independent of n: $\Pi_n \Pi_{l\ \mathrm{even}} p^\dagger_{l+1,n} h^\dagger_{l,n} |0\rangle$ or $\Pi_n \Pi_{l\ \mathrm{odd}} p^\dagger_{l+1,n} h^\dagger_{l,n} |0\rangle$. So there is a twofold-degenerate ground state for $\lambda < 0$ and $|\lambda|$ large, associated with a broken translational symmetry and the development of density wave order of period 2 in the longitudinal direction, in both the quasiparticle and quasihole densities.

The excitation spectrum in the limiting ranges of λ can also be determined as in Sec. II. However, the computations are more involved and we limit ourselves to an analysis of the $\lambda \to \infty$ case in Sec. III A. We will investigate physics at intermediate values of λ in the subsequent subsections, where we will see that the possibilities are richer than the appearance of a single Ising quantum critical point between the states just discussed: Section III B will present a mean-field theory, while Appendixes A and B will discuss continuum quantum field theories which can describe long-wavelength fluctuations near the phase boundaries.

A. Excitations for λ large and positive

There is a large manifold of lowest excited states, all of which have energy $U-E$, in the limit $\lambda \to \infty$. These are the states with exactly one p quasiparticle and one h quasihole, with the particle on the $(D-1)$ dimensional layer $l+1$ and the hole on the layer l. We label these states by

$$|l,n,m\rangle \equiv p^\dagger_{l+1,n} h^\dagger_{l,m} |0\rangle. \tag{3.1}$$

We break the degeneracy between these states by considering corrections in powers of $1/\lambda$. At order $1/\lambda$, the term in the last line in Eq. (1.18) will allow the quasiparticle and the quasihole to hop independently in their own layers, but will not induce any couplings between states with different values of l. The latter appear at order $1/\lambda^2$, when as in Eq. (2.1), a nearest-neighbor dipole pair can hop longitudinally between neighboring layers; again, as in $D=1$, the constraints (1.16) and (1.17) play a crucial role in determining these perturbative corrections. These processes are described by the following effective Hamiltonian for the manifold of excited states with energy $\approx (U-E)$:

$$\begin{aligned}\mathcal{H}_{ph,\mathrm{eff}} = (U-E)\sum_l \Bigg[& \sum_{n,m} |l,n,m\rangle\langle l,n,m| \\ & - \frac{1}{\lambda} \sum_{\langle nm\rangle,k} [n_0 |l,n,k\rangle\langle l,m,k| + (n_0+1)|l,k,n\rangle \\ & \times \langle l,k,m|] + \frac{n_0(n_0+1)}{\lambda^2} \sum_n (|l,n,n\rangle\langle l,n,n| \\ & + |l,n,n\rangle\langle l+1,n,n| + |l+1,n,n\rangle\langle l,n,n|) \Bigg]. \end{aligned} \tag{3.2}$$

Note that the first summation over n,m is unrestricted and ranges independently over the two variables, while the second is over nearest-neighbor pairs $\langle nm\rangle$.

The Hamiltonian $\mathcal{H}_{ph,\mathrm{eff}}$ can be analyzed by the standard techniques of scattering theory. The terms within the first two summations in Eq. (3.2) lead to a ''two-particle'' continuum of quasiparticle and quasihole states, while the terms within the last summation allow these states to scatter and possibly form a dipole bound state. We first form states with total transverse momentum $\mathbf{Q}_\perp$ and relative transverse momentum $\mathbf{q}_\perp$ [these momenta are $(D-1)$-dimensional vectors]:

$$|l,\mathbf{Q}_\perp,\mathbf{q}_\perp\rangle = \frac{1}{N_\perp} \sum_{n,n} e^{i\mathbf{q}_\perp\cdot\mathbf{r}_n + i(\mathbf{Q}_\perp - \mathbf{q}_\perp)\cdot\mathbf{r}_m} |l,n,m\rangle, \tag{3.3}$$

where $N_\perp$ is the number of sites in each layer and $\mathbf{r}_n$ are the spatial positions of the sites. In this basis of states $\mathcal{H}_{ph,\mathrm{eff}}$. Next, we also transform the single longitudinal coordinate l to a ''dipole momentum,'' $q_\parallel$:

$$|q_\parallel,\mathbf{Q}_\perp,\mathbf{q}_\perp\rangle = \frac{1}{N_\parallel} \sum_l e^{iq_\parallel l} |l,\mathbf{Q}_\perp,\mathbf{q}_\perp\rangle. \tag{3.4}$$

In this basis of states, $\mathcal{H}_{ph,\mathrm{eff}}$ takes a form which makes the mapping to standard scattering theory very explicit. The total transverse momentum $\mathbf{Q}_\perp$ and the longitudinal dipole momentum $q_\parallel$ are conserved, while there is scattering between different values of $\mathbf{q}_\perp$:

$$\begin{aligned}\mathcal{H}_{ph,\mathrm{eff}}(\mathbf{Q}_\perp,q_\parallel) = & \sum_{\mathbf{q}_\perp} [\varepsilon_p(\mathbf{q}_\perp) + \varepsilon_h(\mathbf{Q}_\perp - \mathbf{q}_\perp)] |q_\parallel,\mathbf{Q}_\perp,\mathbf{q}_\perp\rangle \\ & \times \langle q_\parallel,\mathbf{Q}_\perp,\mathbf{q}_\perp| + \frac{w^2 n_0(n_0+1)(1+2\cos q_\parallel)}{N_\perp (U-E)} \\ & \times \sum_{\mathbf{q}_\perp,\mathbf{q}'_\perp} |q_\parallel,\mathbf{Q}_\perp,\mathbf{q}_\perp\rangle\langle q_\parallel,\mathbf{Q}_\perp,\mathbf{q}'_\perp|, \end{aligned} \tag{3.5}$$

where (for a hypercubic lattice)

$$\varepsilon_p(\mathbf{q}_\perp) = \frac{(U-E)}{2} - 2w(n_0+1)\sum_\alpha \cos(q_{\perp\alpha}) \tag{3.6}$$

and the summation over α extends over the $D-1$ components of $\mathbf{q}_\perp$. The expression for $\varepsilon_h(\mathbf{q}_\perp)$ is identical to Eq. (3.6) but with n_0+1 replaced by n_0. The Hamiltonian in Eq. (3.5) is that of a particle moving in $D-1$ dimensions with momentum $\mathbf{q}_\perp$ and dispersion $\varepsilon_p(\mathbf{q}_\perp) + \varepsilon_h(\mathbf{Q}_\perp - \mathbf{q}_\perp)$, scattering off a δ-function potential at the origin with strength $w^2 n_0(n_0+1)(1+2\cos q_\parallel)/(U-E)$. Its solution is well known: in addition to the scattering states, a bound state must be present in $D-1=1,2$ for any infinitesimal attractive potential and for strong enough attraction for $D-1>2$. So for the physically relevant cases of $D=2,3$, a bound state must form for a range of $q_\parallel$ values near π. It is clear that the lowest-energy bound state has $\mathbf{Q}_\perp = 0$ and $q_\parallel = \pi$: this is a dipole state, and just as in $D=1$, it is a precursor to the appearance of longitudinal density wave order of period 2. The appearance of this dipole bound state suggests that the first quantum phase transition out of the featureless and

gapped phase present for large positive λ is into a state with Ising charge order; however, our discussion here is for a system with a well-developed gap to quasiparticle and quasihole states, and it is yet not clear whether this approach continues to hold when the gap becomes small—we will return to this question in Appendix A.

B. Mean-field theory

This section will present the results of a mean-field analysis of $\mathcal{H}_{ph}$. The central idea of the mean-field theory is very simple: We treat the quantum fluctuations along the longitudinal direction for all n by the exact numerical treatment developed in Sec. II for $D=1$, while the transverse couplings are treated in a mean-field manner. One important benefit of this approach is that the important constraints (1.16) are treated exactly.

This approach also naturally suggests the appearance of additional phases which have no analog in the $D=1$ case. In particular, the motion of single p and h bosons in the transverse direction implies that superfluid order can develop along these $D-1$ dimensions only. There is no possibility of superfluidity in the longitudinal direction because motion along this direction can occur only via charge neutral dipole pairs which appear in the first term in Eq. (1.18). This *transverse superfluid* therefore has a ''smectic'' character,[12] and its existence implies that we have to allow for $\langle p\rangle$ and $\langle h\rangle$ condensates: These appear naturally in our mean-field theory.

As in the mean-field treatment of the zero-field boson Hubbard model,[6,7] the approximation involves a decoupling of a hopping term. In particular, we only decouple the last transverse hopping term in Eq. (1.18), and obtain the following mean-field Hamiltonian for a set of sites, labeled by l, representing any chain along the longitudinal direction

$$\begin{aligned}\mathcal{H}_{ph,mf}[\langle p_l\rangle,\langle h_l\rangle] &= \sum_l \Big[-wZn_0(\langle h_l\rangle h_l^\dagger + \langle h_l\rangle^* h_l) - wZ(n_0+1)(\langle p_l\rangle p_l^\dagger \\ &\quad + \langle p_l\rangle^* p_l) - w\sqrt{n_0(n_0+1)}(p_{l+1}h_l + p_{l+1}^\dagger h_l^\dagger) \\ &\quad + \frac{(U-E)}{2}(p_l^\dagger p_l + h_l^\dagger h_l) - \mu_l(p_{l+1}^\dagger p_{l+1} - h_l^\dagger h_l)\Big]. \end{aligned} \tag{3.7}$$

Here Z is the coordination number of any site along the $D-1$ transverse directions, and the expectation values $\langle h_l\rangle$ and $\langle p_l\rangle$ have to determined self-consistently from a diagonalization of Eq. (3.7) subject to the constraints associated with Eq. (1.16), which now become

$$p_l^\dagger p_l \leq 1, \quad h_l^\dagger h_l \leq 1, \quad p_l^\dagger p_l h_l^\dagger h_l = 0. \tag{3.8}$$

We have imposed the constraints (1.17) in a mean-field manner by chemical potentials μ_l, whose values must be chosen so that

$$\langle p_{l+1}^\dagger p_{l+1}\rangle = \langle h_l^\dagger h_l\rangle \tag{3.9}$$

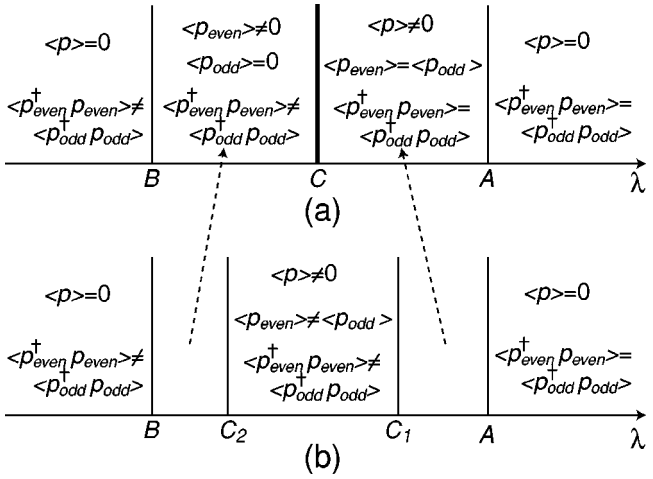

FIG. 10. Schematic phase diagrams as a function of λ. In (a) we display the topology of the phase diagram found by the solution of the mean-field equations: thin lines are second-order quantum phase transitions, while the thick line is a first-order transition. The parity of the l index is indicated as a subscript to the p operators. The expectation values of h quasiholes obey the same relations as those for the p quasiparticles, but with the roles of ''even'' and ''odd'' interchanged. The Ising density wave order is present for all λ to the left of C. In (b) we display a hypothetical phase diagram, possibly induced by fluctuations, in which the first-order transition is replaced by two second-order transitions; now Ising order is present at λ to the left of C_1. There are superfluid-insulator transitions at A, B, C, and C_2 and Ising density wave transitions at C and C_1.

is obeyed; note that these constraints are macroscopic, and so there is no approximation involved in using a chemical potential to impose them. In practice, the diagonalization of $\mathcal{H}_{ph,mf}[\langle p_l\rangle,\langle h_l\rangle]$ must be carried out for a finite number of sites $l=1,\ldots,N$; we found that the mean-field solutions approached the $N=\infty$ limit at quite small and manageable values of N. The ground-state energy of $\mathcal{H}_{ph}$ per chain is not equal to the lowest eigenvalue, E_0, of $\mathcal{H}_{ph,mf}[\langle p_l\rangle,\langle h_l\rangle]$ but is easily computable from it by the relation

$$E_{ph,mf} = E_0 + wZ\sum_l \left[n_0|\langle h_l\rangle|^2 + (n_0+1)|\langle p_l\rangle|^2\right]. \tag{3.10}$$

Indeed, we can also view $\langle p_l\rangle$ and $\langle h_l\rangle$ as arbitrary complex numbers which are determined by the minimization of Eq. (3.10).

The results of the solution of the above mean-field equations are summarized in the schematic phase diagrams in Fig. 10 and in the numerical results in Figs. 11 and 12. It is useful to discuss the phases, in turn, as a function of decreasing λ.

For λ very large and positive (to the right of the point A in Fig. 10), no symmetry is broken, and we have a featureless ground state with no superfluidity and an energy gap to all excitations.

There is a superfluid-insulator transition at A driven by the condensation of the p and h bosons. The superfluidity appears in the direction transverse to the electric field, and all layers behave equivalently. We will examine fluctuations

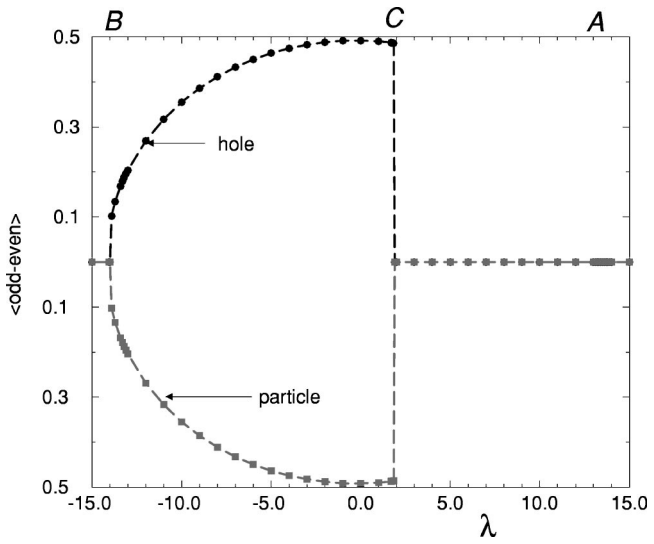

FIG. 11. Mean-field numerical values of the condensates $\langle p_l \rangle$ and $\langle h_l \rangle$ as a function of λ for $n_0=1$ and $Z=4$. The solutions shown are obtained by diagonalizing Eq. (3.7) for $N=6$, but essentially identical results are obtained for $N=4$.

near this critical point in Appendix A and show that the interlayer coupling is irrelevant near the critical point in $D=3$, and so each layer is described by an independent critical theory.

As shown in Fig. 10(a), the mean-field theory exhibits a first-order quantum transition at the the point C associated with the sudden development of Ising density wave order, i.e., the states with λ to the left of C have $\langle p^\dagger_{\rm even} p_{\rm even} \rangle \neq \langle p^\dagger_{\rm odd} p_{\rm odd} \rangle$, and similar for the density of the h bosons. In mean-field theory, the state to the immediate left of C also has the loss of the p condensate in the odd layers (say) and the loss of h condensate in the even layers. In general, it is quite possible that fluctuations, beyond those included in the present mean-field theory, will replace the first-order transition at C by two second-order transitions at C_1 and C_2, as shown in Fig. 10(b). At the first transition at C_1, the order parameter is only the Ising density wave, while there is p and h transverse superfluidity in all layers; the second transition at C_2 involves the continuous vanishing of the p (h) condensate in the odd (even) layers in a superfluid-insulator transition, in the presence of a background of Ising density wave order.

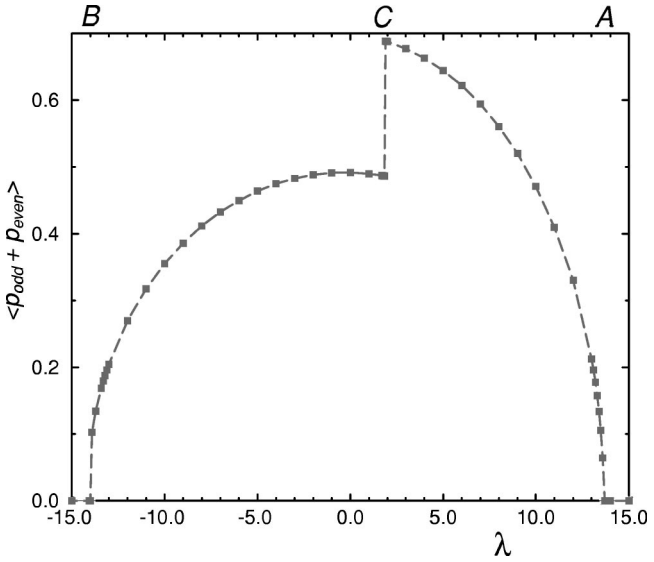

FIG. 12. As in Fig. 11. The values of $\langle h_{\rm odd} + h_{\rm even} \rangle$ are very close, but not identical, to the p values shown above.

The final transition at the point B involves loss of all p and h condensates. There is long-range Ising density wave order at all λ to the left of B, and a gap to all excitations.

The theory of fluctuations about these mean-field results is discussed in Appendixes A and B. As we have already noted, these could be strong enough to also modify the topology of the phase diagram in Fig. 10(a). One extreme possibility is that the transverse superfluid phases could disappear entirely, and we are left only with two insulating phases, one with Ising density wave order and the other without; the phase diagram is then as in $D=1$. However, we show in Appendix A that the value of a particular critical exponent determines that this is not the generic situation.

IV. OTHER FIELD ORIENTATIONS AND LATTICES

Our discussion has so far limited itself to hypercubic lattices, with the direction of the electric field **e** oriented along one of the principal axes. Similar analyses can be carried out for other lattices and for other directions of **e**. A large variety of correlated phases appear possible, including many not related to those already discussed. We will illustrate these possibilities by an example here, but leave a more detailed discussion to future work.

Consider a square lattice (in $D=2$) but with $\mathbf{e}=(1,1)$. In this case, the resonant transitions from the Mott insulator involve moving a b_i boson by one lattice spacing, either along the $+x$ or $+y$ direction. However, once such a dipole has been created, the quasiparticle and the quasihole cannot move resonantly to any other sites (except by processes of order w^2/U which we have consistently neglected here). So the resonant subspace can be described completely in terms of dipole states, just as in the $D=1$ case discussed earlier. A typical state is illustrated in Fig. 13. The effective Hamiltonian of this space of dipole resonant states is identical in form to Eq. (1.12):

$$\mathcal{H}'_d = -w\sqrt{n_0(n_0+1)}\sum_a (d_a + d_a^\dagger) + (U-E)\sum_a d_a^\dagger d_a , \tag{4.1}$$

except now the label a extends over the links of the square lattice. There continues to be a hard-core constraint $d_a^\dagger d_a \leqslant 1$ like Eq. (1.10), but the possibility for new physics arises from the complexity of the generalization of the constraint (1.11), which is now

$$d_a^\dagger d_a d_b^\dagger d_b = 0 \quad \text{for links } a,b \text{ which share a common site.} \tag{4.2}$$

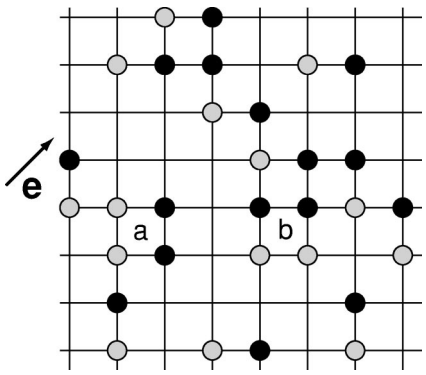

FIG. 13. A typical state in the resonant subspace for a square lattice with $\mathbf{e}=(1,1)$. Representation is as in Fig. 5. The quasiparticles and quasiholes occur only occur in dipoles oriented along the $+x$ or $+y$ directions. Note that it is possible for dipoles to undergo a ring exchange around a plaquette, in which the configuration around plaquette *a* can become like that around plaquette *b*; this process is contained in the resonant model $\mathcal{H}_d'$ in Eqs. (4.1) and (4.2) and does *not* require much weaker virtual processes in the Hubbard model $\mathcal{H}$ (which are suppressed by powers of w/U).

Note that each dipole blocks the occupancy of dipoles on six neighboring links. It would be interesting to determine the properties of $\mathcal{H}_d'$ subject to the constraint (4.2).

The possibility of rich physics becomes apparent in thinking about the case $\lambda<0$ and $|\lambda|$ large. Here the low-lying manifold of states corresponds to maximizing the number of dipoles, and these are in one-to-one correspondence with the close-packed dimer coverings of the square lattice. A natural ring-exchange term of the dipole bosons also becomes apparent upon considering perturbative corrections in powers of $1/|\lambda|$: this derivation is similar in spirit to that in Sec. II (see Fig. 13). We emphasize that the dominant ring exchange does not come from virtual higher-order processes in the underlying Hubbard model $\mathcal{H}$ (which are strongly suppressed by factors of w/U), but is already contained within the physics of the resonant subspace as described by Eqs. (4.1) and (4.2). In analogy with other studies of quantum dimer models[13–15] and boson ring-exchange models, possibilities of bond-ordered phases open up. Fractionalized and Bose metal phases[16] are also possible, but these may be more likely on nonbipartite lattices.

We close by noting that it is easily possible to orient **e** so that only one direction is resonant. For a cubic lattice in $D=3$ this can be done by choosing $\mathbf{e}=(1,a,b)$ where $a,b\neq 0,1$ are some arbitrary real numbers. Then resonant transitions to dipole states can occur only along the x direction, and the resonant manifold separates into decoupled one-dimensional systems, each of which is separately described by the one-dimensional (1D) dipole Hamiltonian $\mathcal{H}_d$ in Eq. (1.12). This may be a simple way of experimentally realizing the model $\mathcal{H}_d$.

V. IMPLICATIONS FOR EXPERIMENTS

An important issue that must be faced at the outset is the extent to which the nonequilibrium time-dependent experiments can be described by the ground and low-energy states of the effective models that have been discussed in this paper. In the experiments of Greiner *et al.*,[2] the "electric field" (in practice, this is realized by a magnetic field gradient) is turned from an initial zero value to E in a time of order h/w. In a system under the conditions (1.1), this may not allow easy access of the ground state. As an alternative, we suggest that E be ramped up rapidly to a value to the right of the point A in Fig. 10, and then slowly increased through the possible critical points in Fig. 10. This could produce states with either the density wave Ising order, or the transverse superfluid order.

Having produced such states, the next challenge is to directly detect the quantum order parameters associated with the phases in Fig. 10. We address two possible probes in the subsections below.

A. Momentum distribution

One experimental quantity that is relatively easy to measure is the momentum distribution of the atoms contained in the optical lattice. This is done by shutting off the lattice potential and the trapping potential and allowing the atoms to freely expand until the resulting cloud is large enough that its density profile can be spatially resolved optically. The scale to which the cloud expands before measurement can be made much larger than the original lattice dimensions. In this limit the final spatial position at which an atom is detected determines the momentum at which the momentum distribution function is being measured.

The momentum distribution for the boson Hubbard model containing N sites is given by

$$\Pi(\mathbf{q})=|f(\mathbf{q})|^2\frac{1}{N}\sum_{j,k}e^{i\mathbf{q}\cdot(\mathbf{r}_j-\vec{\mathbf{r}}_k)}\langle b_j^\dagger b_k\rangle, \tag{5.1}$$

where $f(\mathbf{q})$ is the form factor for the tight-binding orbitals associated with the lattice potential and the momentum $\mathbf{q}=m\mathbf{R}/(\hbar t_{ex})$, where $\mathbf{R}$ is the distance from the detection position to the center of the trap, m is the mass of the atoms, and t_{ex} is the time elapsed in the expansion (this expression ignores the influence of gravity, but an appropriate modification is straightforward). The development of off-diagonal long-range order peaks the momentum distribution at the values of $\mathbf{q}$ equal to the reciprocal lattice vectors of the optical lattice potential and has been used as an experimental signature of the superfluid phase.[1,2]

Let us first consider the $D=1$ case. A very important consequence of our restriction to the subspace of resonant states is that the boson correlator $\langle b_l^\dagger b_{l'}\rangle$ vanishes for $|l-l'|>1$. Hence Eq. (5.1) becomes (q is the component of $\mathbf{q}$ in the direction of the "electric" field)

$$\Pi_{1D}(q)=|f(q)|^2\left[n_0+\frac{\sqrt{n_0(n_0+1)}}{2}\times\sum_l\{e^{iq}\langle d_l^\dagger\rangle+e^{-iq}\langle d_l\rangle\}\right], \tag{5.2}$$

where the lattice spacing has been taken to be unity, and $d_l^\dagger$ is the dipole creation operator defined in Eq. (1.9). For the

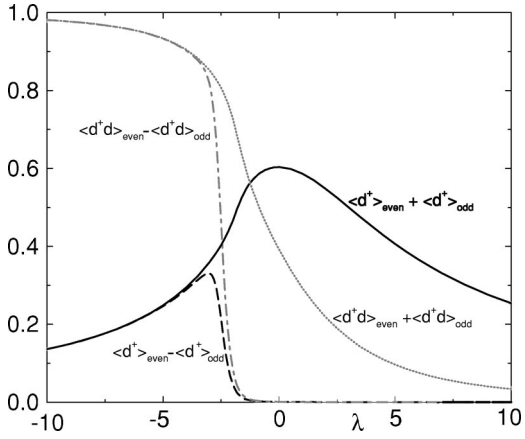

FIG. 14. Ground state expectation values of $\langle d_l \rangle$ and $\langle d_l^\dagger d_l \rangle$ for the $D=1$ model $\mathcal{H}_d$ in (1.12). The results are for $N=16$ sites and periodic boundary conditions. A very small ordering field was applied to choose one of the degenerate Ising ground states present for sufficiently negative λ. We have chosen the gauge in which $\langle d \rangle$ are real.

periodic boundary conditions we have used (as we noted earlier, such boundary conditions are not physical, but they should not modify the results in the limit of large system sizes), the values of $\langle d_l \rangle$ depend only on the parity of l (a very small ordering field is applied to lift the Ising symmetry, and we choose one of the ground states in the region with spontaneous Ising order), and hence the overall amplitude of Eq. (5.2) is determined only by $\langle d_{\rm even} \rangle + \langle d_{\rm odd} \rangle$. We show our numerical results for these and other related quantities for the Hamiltonian $\mathcal{H}_d$ in Eq. (1.12) in Fig. 14. There is a broad maximum in $\langle d_{\rm even} \rangle + \langle d_{\rm odd} \rangle$ near the Ising critical point, as this is the region with the maximal dipole number fluctuations. The critical singularity in this quantity at $\lambda = \lambda_c$ is determined by that of the energy operator of the Ising field theory: this singularity is weak and is essentially unobservable in Fig. 14. The quantities sensitive to the Ising order parameter (such as $\langle d_{\rm even} \rangle - \langle d_{\rm odd} \rangle$) show more singular behavior in Fig. 14 near λ_c determined by the magnetization exponent β. However, these observables are not detectable by a measurement of the momentum distribution function.

In higher dimensions ($D>1$) for the case where **e** is aligned along one of the lattice directions, the dependence of the distribution function on $q_\parallel$ should be qualitatively similar to the q dependence in the $D=1$ case discussed above. However, a much clearer signal of the transverse superfluidity should be visible. The presence of the $\langle p \rangle$ and $\langle h \rangle$ condensates implies that the correlator (5.1) has phase-coherent contributions when $\mathbf{r}_j - \mathbf{r}_k$ lies in the plane perpendicular to the applied ''electric'' field. This implies that in states with transverse superfluidity, there should be Bragg peaks along *lines in* $\mathbf{q}$ *space* with values of $\mathbf{q}_\perp$ equal to the reciprocal lattice vectors of the $(D-1)$-dimensional lattice lying in the plane perpendicular to **e**. As the transverse dimensionality is $D-1=2$, the superfluid order can only be quasi long range at nonzero temperature, and hence the Bragg peaks are not true δ functions in the infinite-volume limit, but are power-law singularities. Experimental detection of these Bragg lines would be quite interesting.

B. Ising order parameter

We have seen that the Ising order is not directly reflected in the momentum distribution and hence cannot be measured in the free expansion method described above. The properties of the Ising order parameter ϕ are discussed in Appendix B; one convenient definition for ϕ is

$$\phi = \frac{1}{N} \sum_l (-1)^l \langle d_l^\dagger d_l \rangle \tag{5.3}$$

in $D=1$ [see Eq. (2.3)], and a related definition can be made for higher D. One possibility for coupling to the Ising order parameter experimentally would be to introduce a phase-locked subharmonic standing wave at half the wave vector of the optical lattice so that the standing wave takes the form (in 1D)

$$\Phi(x,t) \propto [\cos(Qx)\cos(Qct) + B\cos(Qx/2+\theta)\cos(Qct/2)]. \tag{5.4}$$

Squaring this and taking the time average gives the effective lattice potential

$$V(x) \propto -[\cos^2(Qx) + B^2\cos^2(Qx/2+\theta)]. \tag{5.5}$$

Adjusting the relative phase to $\theta=0$ or $\pi/2$ adds a ''staggered magnetic field'' term to the Ising Hamiltonian

$$H_B \propto \pm B^2 \phi. \tag{5.6}$$

A simpler experimental method for the case where the trap confinement is strong in the directions transverse to the axis of the 1D lattice is the following. An additional standing wave (derived from the same laser) but oriented in the y direction (say) would yield

$$\Phi(x,y=0,t) \propto [\cos(Qx)\cos(Qct) + B\cos(Qct)] \tag{5.7}$$

and hence a potential along the x axis of

$$V(x,y=0) \propto -[\cos^2(Qx) + 2B\cos(Qx) + B^2], \tag{5.8}$$

which would also couple to the Ising order

$$H_B \propto B\phi. \tag{5.9}$$

In either case, such a perturbation could be used to break the Ising symmetry and selectively populate one of the two Ising states. In addition, it could be used to *measure* the order parameter itself. The ac Stark shift of the atomic hyperfine levels would differ between adjacent sites. The relative strengths of the split hyperfine absorption lines would then be a measure of the Ising order parameter.[17]

ACKNOWLEDGMENTS

The authors thank Immanuel Bloch and Mark Kasevich for numerous valuable discussions of their experiments. This research was supported by U.S. NSF Grant Nos. DMR 0098226 and DMR 0196503.

APPENDIX A: FLUCTUATIONS AND QUANTUM FIELD THEORIES: SUPERFLUID-INSULATOR TRANSITIONS

The mean-field theory of Sec. III B can be used as a starting point for a more sophisticated treatment of fluctuations. Such fluctuations will modify the mean-field exponents in the vicinity of the second-order phase boundaries in Fig. 10(a), but could also change the topology of the phase diagram to that in Fig. 10(b).

We analyze fluctuations about the mean-field results using a method very similar to that described in Chap. 10 of Ref. 11 for the Hubbard model. We decouple the *intra*layer hopping terms in $\mathcal{H}_{ph}$ [those in the last line of Eq. (1.18)] only by Hubbard-Stratonovich transformations using complex fields $P_l(\mathbf{r}_\perp,\tau)$ and $H_l(\mathbf{r}_\perp,\tau)$ where $\mathbf{r}_\perp$ is a spatial coordinate for the $D-1$ transverse directions and τ is imaginary time. Then, after standard simplifications, we obtain an expression for the partition function $\mathcal{Z}_{ph}$ of $\mathcal{H}_{ph}$ which has the following schematic form:

$$\mathcal{Z}_{ph}=\int \mathcal{D}P_l(\mathbf{r}_\perp,\tau)\mathcal{D}H_l(\mathbf{r}_\perp,\tau) \times\exp\left[-\int d^{D-1}\mathbf{r}_\perp(\mathcal{S}_0+\mathcal{S}_1)\right]. \tag{A1}$$

The action $\mathcal{S}_0$ involves couplings only within a single layer l, but with different values of $\mathbf{r}_\perp$,

$$\mathcal{S}_0\equiv\int d\tau\sum_l\ [K_p|\nabla_\perp P_l(\mathbf{r}_\perp,\tau)|^2+r_p|P_l(\mathbf{r}_\perp,\tau)|^2 +K_h|\nabla_\perp H_l(\mathbf{r}_\perp,\tau)|^2+r_h|H_l(\mathbf{r}_\perp,\tau)|^2], \tag{A2}$$

and $K_{p,h}$, $r_{p,h}$ are coupling constants. Note that the factors of n_0 and n_0+1 in the last line of Eq. (1.18) break particle-hole symmetry and so there is no special symmetry relation between these coupling constants. The action $\mathcal{S}_1$ couples different layers and times together for the same value of $\mathbf{r}_\perp$:

$$e^{-\mathcal{S}_1}\equiv\int \mathcal{D}p_l(\tau)\mathcal{D}h_l(\tau)\mathcal{P}[p_l(\tau),h_l(\tau)] \times\exp\left[-\int d\tau\left\{\sum_l\ \left(p_l^\dagger\frac{\partial p_l}{\partial\tau}+h_l^\dagger\frac{\partial h_l}{\partial\tau}\right) +\mathcal{H}_{ph,mf}[P_l(\mathbf{r}_\perp,\tau),H_l(\mathbf{r}_\perp,\tau)]\right\}\right], \tag{A3}$$

with $\mathcal{H}_{ph,mf}$ defined in Eq. (3.7), and $\mathcal{P}$ is a projection operator which represents the constraints (3.8) (these could be imposed formally in the functional integral by a very strong on-site repulsive interaction among the p_l and h_l bosons). As in Sec. III B, we have imposed the constraints (1.17) by time-independent Lagrange multipliers (''chemical potentials'') μ_l: As we noted earlier, there is no approximation involved in neglecting the fluctuations of μ_l, because there is only one constraint per layer and there are a macroscopic number of particles within each layer. The values of μ_l are to be determined at the end by the requirements

$$\frac{\partial\ln\mathcal{Z}_{ph}}{\partial\mu_l}=0. \tag{A4}$$

Further progress in describing the properties of $\mathcal{Z}_{ph}$ requires some understanding of the structure of $\mathcal{S}_1$. This was already addressed to some extent in Sec. III B where we explored the properties of the Hamiltonian $\mathcal{H}_{ph,mf}$. However, here we need to generalize that analysis to the case where its arguments are time-dependent fields $P_l(\mathbf{r}_\perp,\tau)$ $H_l(\mathbf{r}_\perp,\tau)$. This is quite an involved task, but we will only need some general constraints that are placed on the structure of $\mathcal{S}_1$ by the principles of gauge invariance. In particular, associated with the conservation laws (1.17), we observe that $\mathcal{Z}_{ph}$ is invariant under the time- and layer-dependent transformations generated by the arbitrary field $\phi_l(\tau)$:

$$\begin{aligned} p_{l+1}&\to p_{l+1}e^{i\phi_l(\tau)},\\ h_l&\to h_l e^{-i\phi_l(\tau)},\\ P_{l+1}&\to P_{l+1}e^{i\phi_l(\tau)},\\ H_l&\to H_l e^{-i\phi_l(\tau)},\\ \mu_l&\to\mu_l+i\frac{\partial\phi_l}{\partial\tau}. \end{aligned} \tag{A5}$$

We are interested here only in the case of time-independent μ_l, and so this transformation takes μ_l into an unphysical set of values; nevertheless, as we will see shortly, Eq. (A5) is still useful in placing constraints on $\mathcal{S}_1$ in the physical regime.

First, we address the influence of fluctuations by approaching the transition involving condensation of P_l, H_l from the side of large and positive λ; i.e., we increase E (and decrease λ) until mean-field theory indicates we are approaching a phase with transverse superfluidity at the point A in Fig. 10. The ground state of $\mathcal{H}_{ph,mf}$ is translationally invariant in this region, and so we can safely assume that all the coupling constants in $\mathcal{S}_1$ are also independent of l. Similarly, we can assume that μ_l is also independent of l. If we were to approach the condensation of P_l, H_l from the opposite side of negative λ, the ground state of $\mathcal{H}_{ph,mf}$ would have a broken Ising symmetry, and the following analysis would only need to be modified by allowing all couplings, and μ, to depend upon the l sublattice. We describe the action $\mathcal{S}_1$ by expanding it in powers of the fields P_l, H_l and in their temporal gradients (the $\mathbf{r}_\perp$ and τ dependence of these fields is now implicit); to second order in the fields and to first order in temporal gradients, the most general terms invariant under Eqs. (A5) are

$$\mathcal{S}_1=\sum_l\ \int d\tau\left[\tilde{K}_p P_l^*\frac{\partial P_l}{\partial\tau}+\tilde{K}_h H_l^*\frac{\partial H_l}{\partial\tau} +\tilde{K}_{ph}\left(P_{l+1}\frac{\partial H_l}{\partial\tau}+P_{l+1}^*\frac{\partial H_l^*}{\partial\tau}\right)+\tilde{r}_p|P_l|^2+\tilde{r}_h|H_l|^2 +\tilde{r}_{ph}(P_{l+1}H_l+P_{l+1}^*H_l^*)\right]. \tag{A6}$$

Consistently requiring invariance of Eq. (A6) under the time-dependent gauge transformations (A5) to the order we have performed the expansion in $\mathcal{S}_1$ demands additional constraints on the coupling constants above; these are

$$\tilde{K}_p = -\frac{\partial \tilde{r}_p}{\partial \mu}, \quad \tilde{K}_h = \frac{\partial \tilde{r}_h}{\partial \mu}, \quad \tilde{K}_{ph} = \frac{\partial \tilde{r}_{ph}}{\partial \mu}. \tag{A7}$$

There are also a large number of permitted higher-order terms in $\mathcal{S}_1$ which we have not written down explicitly; some of these will play an important role below.

Armed with the low-order terms in the action $\mathcal{S}_0 + \mathcal{S}_1$ controlling the fluctuations of P_l and H_l we can now use standard techniques to focus on the low-energy excitations. It is natural to diagonalize the quadratic form displayed in these actions: this will lead to two eigenmodes with distinct eigenvalues. We focus attention on the lower eigenmode, while integrating out the higher eigenmode. We identify the lower eigenmode by the field Ψ_l: this has the structure

$$\Psi_l(\mathbf{r}_\perp, \tau) = c_p P_{l+1}(\mathbf{r}_\perp, \tau) + c_h H_l^*(\mathbf{r}_\perp, \tau) \tag{A8}$$

for some constants $c_{p,h}$. Note that we are performing the same "rotation" in field space for all $\mathbf{r}_\perp$ and τ (and hence all frequencies). This ensures that Ψ_l has a simple behavior under Eqs. (A5):

$$\Psi_l \to \Psi_l e^{i\phi_l(\tau)}. \tag{A9}$$

We integrate out the high-energy mode orthogonal to Eq. (A8) and obtain our final effective action now expressed in terms of Ψ_l:

$$\mathcal{Z}_{ph} = \int \mathcal{D}\Psi_l(\mathbf{r}_\perp, \tau) \exp\left[-\int d^{D-1}\mathbf{r}_\perp d\tau \sum_l (\mathcal{L}_0 + \mathcal{L}_1) \right],$$

$$\mathcal{L}_0 = |\nabla_\perp \Psi_l|^2 + \left| \frac{\partial \Psi_l}{\partial \tau} \right|^2 + r_\psi |\Psi_l|^2 + \frac{u}{2}|\Psi_l|^4 + v|\Psi_l|^2 |\Psi_{l+1}|^2,$$

$$\mathcal{L}_1 = K_\psi \Psi_l^* \frac{\partial \Psi_l}{\partial \tau}. \tag{A10}$$

We have rescaled Ψ_l and time to obtain unit coefficients for the first two terms in $\mathcal{L}_0$, and the $\mathbf{r}_\perp$ dependence of Ψ_l is implicit. We have also written down a quartic nonlinearity within a layer (u) and the simplest coupling between neighboring layers (v) which preserves invariance under Eq. (A9); we expect both these couplings to be positive because of the repulsive interactions between the microscopic bosonic degrees of freedom. The parameter r_ψ tunes the system across the quantum phase transition at the point A in Fig. 10 which resides at $r_\psi = r_{\psi c}$; the transition is from the featureless, gapped phase at large positive λ ($r_\psi > r_{\psi c}$) to a phase with superfluidity in the transverse $D-1$ dimensions as λ is decreased ($r_\psi < r_{\psi c}$); the superfluidity is associated with the condensation of Ψ_l.

Just as in the derivation of Eqs. (A7), we can also examine the consequences of time-dependent gauge transformations in Eqs. (A5) and (A9) on Eqs. (A10). This now leads to the relationship

$$K_\psi = -\frac{\partial r_\psi}{\partial \mu}. \tag{A11}$$

Combined with Eq. (A4), the above result now yields a crucial result. Close to the quantum critical point, the singular free energy associated with $\mathcal{Z}_{ph}$ is determined directly by r_ψ. For this singular term to obey Eq. (A4), we conclude (as also argued in Chap. 10 of Ref. 11) that $\partial r_\psi / \partial \mu = 0$ at $r_\psi = r_{\psi c}$; Eq. (A11) now implies

$$K_\psi = 0 \quad \text{at} \quad r_\psi = r_{\psi c}. \tag{A12}$$

So we can neglect $\mathcal{L}_1$, and the critical theory is described entirely by $\mathcal{L}_0$. Within each layer l, this theory has the relativistic invariance of $(D-1)+1$ spacetime dimensions and dynamic critical exponent $z=1$.

Before turning to an examination of the properties of Eqs. (A10), we pause to discuss the modifications required to describe the onset of transverse superfluidity with increasing λ in the region $\lambda < 0$ at the point B in Fig. 10 [a similar reasoning can also be applied to the point C_2 in Fig. 10(b)]. Here, long-range Ising order is already present in $H_{ph,mf}$ for λ sufficiently negative. We can proceed to a description of the superfluid transition as above, but as noted earlier, all couplings in Eqs. (A10) will acquire an l dependence which modulates with period 2. The tuning parameter r_ψ will also be different for even and odd l. Consequently only Ψ_l with l even (say) will become critical near the transition, while Ψ_l with l odd remains noncritical and can be integrated out. The simplest interlayer coupling between critical modes is now $|\Psi_l|^2 |\Psi_{l+2}|^2$, but its coefficient should be small and is likely to be attractive.

We now return to an examination of Eqs. (A10) for the case of l-independent couplings at the transition with $U-E$ positive at the point A in Fig. 10. It remains to examine the consequences of the interlayer coupling v on the standard theory of the superfluid-insulator transition. At $v=0$, we have the standard φ^4 field theory with O(2) symmetry in $(D-1)+1=D$ spacetime dimensions. As a first step, we can compute the scaling dimension of v at its critical point. A standard power-counting argument shows that

$$\dim[v] = \frac{2}{\nu} - D = \frac{\alpha}{\nu}, \tag{A13}$$

where ν and α are the standard correlation length and "specific heat" exponents in D spacetime dimensions. In $D=3$, the O(2) fixed point has[18] $\alpha = -0.015 < 0$, and so we conclude that v is formally irrelevant. In $D=2$, the very weak specific heat singularity at the Kosterlitz-Thouless transition suggests the same conclusion.

A more complete analysis of the influence of v can be obtained by considering a physical susceptiblity for ordering in the longitudinal direction. As we have seen in Secs. II and III B, the simplest allowed ordering is a density wave of period 2. The tendency to this ordering is measured by the static susceptibility χ_π:

$$\chi_\pi = \frac{1}{N_\parallel}\sum_{l,l'}\int d^{D-1}\mathbf{r}_\perp d\tau(-1)^{l+l'} \times \langle |\Psi_l(\mathbf{r}_\perp,\tau)|^2 |\Psi_{l'}(\mathbf{0},0)|^2\rangle. \quad \text{(A14)}$$

Note that this response function is similar to S_π in Eq. (2.3), but we are considering here a zero frequency response, while Eq. (2.3) involved an equal-time correlator. We can compute Eq. (A14) in powers of v and, by a familiar Dyson-type argument, write it as

$$\chi_\pi = \frac{\mathcal{C}}{1-2v\mathcal{C}}, \quad \text{(A15)}$$

where $\mathcal{C}$ is an ''irreducible'' correlator within a single layer (it is irreducible with respect to cutting a v interaction line):

$$\mathcal{C} = \int d^{D-1}\mathbf{r}_\perp d\tau \langle |\Psi_l(\mathbf{r}_\perp,\tau)|^2 |\Psi_l(\mathbf{0},0)|^2\rangle. \quad \text{(A16)}$$

The computation leading to Eqs. (A15) and (A16) is the field-theoretic analog of the computations which lead to a dipole bound state induced by the interlayer coupling in the strong-coupling analysis of Sec. III A. Ignoring the influence of v on $\mathcal{C}$, standard scaling arguments imply that $\mathcal{C}$ has a singular part which behaves as

$$\mathcal{C} \sim |r_\psi - r_{\psi c}|^{-\alpha}. \quad \text{(A17)}$$

If we had $\alpha > 0$, then the denominator in Eq. (A15) would vanish at some $r_\psi > r_{\psi c}$ for any small v, and χ_π would then diverge: this would imply the presence of an Ising density wave transition before the onset of superfluidity. However, $\alpha < 0$ in $D=3$, and so this condition does not apply. Nevertheless, there is a significant (albeit finite) enhancement of the specific near the O(2) critical point in $D=3$, and so the instability in χ_π may well occur for a moderate value of v. If so, the mean-field phase diagram would be modified, and the Ising ordered phase would fully overlap and extend beyond the region with transverse superfluidity. Indeed, under suitable conditions, the superfluid phase could also shrink to zero, and we would then have only a single Ising transition between two insulating phases. Alternatively, if the Ising fluctuations are weaker, χ_π could diverge somewhere in the superfluid phase to the left of A in Fig. 10, and then the mean-field phase diagram would be modified to the structure in Fig. 10(b).

APPENDIX B: ISING PHASE TRANSITION

In Appendix A we completed a description of fluctuations near all the superfluid-insulator transitions in Fig. 10. It remains to describe the second-order Ising critical point C_1 in Fig. 10(b); this we do in the present appendix.

As usual, we expect the Ising phase transition to be realized by a quantum field theory of a real scalar field $\phi(\mathbf{r},\tau)$, where $\mathbf{r}=(l,\mathbf{r}_\perp)$ is a D-dimensional spatial coordinate. The main subtlety here is that the Ising transition occurs in a background of transverse superfluid order, and corrections from superflow fluctuations can lead to anisotropic singular corrections to the critical theory. A theory of an Ising order parameter coupled to isotropic superflow fluctuations has been analyzed by Frey and Balents;[19] here, we will show that the particular anisotropic nature of both the superfluid and Ising order leads to a more singular coupling between the two order parameters.

Any observable sensitive to the period-2 modulation in the density of particles or holes can be used to define the order parameter $\phi(\mathbf{r},\tau)$. A convenient choice in our present continuum formulation is to take

$$\phi(l,\mathbf{r}_\perp,\tau) \sim (-1)^l |\Psi_l(\mathbf{r}_\perp,\tau)|^2. \quad \text{(B1)}$$

An effective action $\mathcal{S}_\phi$ for the Ising field ϕ can be generated by using ϕ as a Hubbard-Stratonovich field to decouple the v term in Eqs. (A10). This leads to an action with the structure

$$\mathcal{S}_\phi = \int d^D\mathbf{r}d\tau\left[\frac{1}{2}(\partial_\tau\phi)^2 + \frac{K_\perp}{2}(\nabla_\perp\phi)^2 + \frac{K_\parallel}{2}(\nabla_\parallel\phi)^2 + u_I\phi^4\right] - w_I\sum_l \int d^{D-1}\mathbf{r}_\perp d\tau(-1)^l |\Psi_l(\mathbf{r}_\perp,\tau)|^2 \phi(l,\mathbf{r}_\perp,\tau), \quad \text{(B2)}$$

where the fluctuations of Ψ_l are described by Eqs. (A10) and we have included the usual analytic terms present in the ϕ^4 theory of an Ising quantum critical point. The last term in Eq. (B2) represents a linear coupling between the Ising order parameter and density fluctuations in the superfluid state. In the isotropic case considered by Frey and Balents such a linear coupling was absent, and the simplest allowed coupling was between ϕ^2 and the density fluctuations: this was because the Ising order parameter represented a density wave at a large wave vector, and they coupled linearly only to fluctuations of the superfluid phase at the same wave vector, and the latter are quite high energy. In the present case, also, the $(-1)^l$ factor in the last term in Eq. (B2) also shows that ϕ couples linearly to the superfluid phase fluctuations at a wave vector $q_\parallel = \pi$. However, the key difference here is that the superfluidity is present only along the transverse direction, and to leading order, the superfluid phase fluctuations are *independent* of $q_\parallel$.

The singular effect of the w_I term in Eq. (B2) can be illustrated by integrating out the Ψ_l using the action (A10) in a single-loop approximation. To leading order in u, we are in the transverse superfluid state as long as $r_\psi < 0$, and a simple calculation of the phase and amplitude fluctuations of the superfluid order parameter shows that we generate the following term in $\mathcal{S}_\phi$:

$$\frac{1}{2u}\sum_{q_\parallel,\mathbf{q}_\perp,\omega} |\phi(q_\parallel,\mathbf{q}_\perp,\omega)|^2 \frac{|r_\psi|(\mathbf{q}_\perp^2+\omega^2)}{|r_\psi|(\mathbf{q}_\perp^2+\omega^2) + K_\psi^2\omega^2/2}, \quad \text{(B3)}$$

where ω is an imaginary frequency. Note that this is a singular function of $\mathbf{q}_\perp$ and ω only when $K_\psi \neq 0$. We do not expect $K_\psi = 0$ near the Ising critical point, because exact particle-hole symmetry is not present in the underlying Hamiltonian, and the arguments which lead to Eq. (A12)

hold only at the superfluid-insulator transition. All the couplings in $\mathcal{S}_\phi$ can be expected to be a smooth function of μ, and the constraint is now expected to lead only to a Fisher renormalization[20] of exponents. An analysis of $\mathcal{S}_\phi$ with Eq. (B3) included requires a renormalization group computation: this we leave to future work, as a full discussion of the renormalization of the momentum dependence of the propagator requires a two-loop analysis.

In closing, we note that although $K_\psi \neq 0$, in practice the degree of particle-hole symmetry breaking is quite small, as indicated by the almost equal values of $\langle p \rangle$ and $\langle h \rangle$ in Figs. 11 and 12. So K_ψ can also be expected to be quite small, and we should, therefore, also consider the case $K_\psi = 0$. In this case, Eq. (B3) does not induce any singular terms, and we have to consider terms induced by Ψ_l fluctuations at higher orders in u and also the term included in Ref. 19.

*Electronic address: subir.sachdev@yale.edu; URL: http://pantheon.yale.edu/ subir
†Electronic address: k.sengupta@yale.edu
‡Electronic address: steven.girvin@yale.edu; URL: http://pantheon.yale.edu/~smg47

[1] C. Orzel, A.K. Tuchman, M.L. Fenselau, M. Yasuda, and M.A. Kasevich, Science **291**, 2386 (2001).
[2] M. Greiner, O. Mandel, T. Esslinger, T.W. Hänsch, and I. Bloch, Nature (London) **415**, 39 (2002).
[3] C.I. Duruöz, R.M. Clarke, C.M. Marcus, and J.S. Harris, Jr., Phys. Rev. Lett. **74**, 3237 (1995).
[4] A.A. Middleton and N.S. Wingreen, Phys. Rev. Lett. **71**, 3198 (1993).
[5] If we ignore the spin of the fermions (as may be the justified under certain physical conditions, such as the presence of a magnetic field), then the generalization of our results to fermionic Mott insulators (which must have $n_0 = 1$) is relatively straightforward. The $D = 1$ results apply unchanged to fermionic Mott insulators. For $D > 1$, the Hamiltonian H_{ph} in Eq. (1.18) applies unchanged, but with p and h fermionic operators. The first two constraints in Eq. (1.16) are now automatically accounted for by fermionic statistics, while the last must be implemented by an infinite local repulsion between quasiparticles and quasiholes. Gapped phases appear for large $|\lambda|$ (the region with $\lambda \ll 0$ having Ising density wave order), but the particle-hole hopping asymmetry allows this fermionic model to exhibit gapless Fermi surfaces for motion in the transverse direction. The case of spinful fermions will have an even richer behavior, driven by the antiferromagnetic coupling between the spins.
[6] M.P.A. Fisher, P.B. Weichman, G. Grinstein, and D.S. Fisher, Phys. Rev. B **40**, 546 (1989).
[7] D. Jaksch, C. Bruder, J.I. Cirac, C.W. Gardiner, and P. Zoller, Phys. Rev. Lett. **81**, 3108 (1998).
[8] T.D. Kuhner, S.R. White, and H. Monien, Phys. Rev. B **61**, 12 474 (2000).
[9] J. Zapata, A.M. Guzmán, M.G. Moore, and P. Meystre, Phys. Rev. A **63**, 023607 (2001).
[10] J.H. Davies and J.W. Wilkins, Phys. Rev. B **38**, 1667 (1998).
[11] S. Sachdev, *Quantum Phase Transitions* (Cambridge University Press, Cambridge, England, 1999).
[12] S.A. Kivelson, E. Fradkin, and V.J. Emery, Nature (London) **393**, 550 (1998).
[13] D.S. Rokhsar and S.A. Kivelson, Phys. Rev. Lett. **61**, 2376 (1988).
[14] N. Read and S. Sachdev, Phys. Rev. B **42**, 4568 (1990); S. Sachdev, *ibid.* **45**, 12 377 (1992).
[15] R. Moessner and S.L. Sondhi, Phys. Rev. Lett. **86**, 1881 (2001).
[16] A. Paramekanti, L. Balents, and M.P.A. Fisher, cond-mat/0203171 (unpublished).
[17] We are grateful to Mark Kasevich for this suggestion.
[18] M. Campostrini, A. Pelissetto, P. Rossi, and E. Vicari, Phys. Rev. B **61**, 5905 (2000).
[19] E. Frey and L. Balents, Phys. Rev. B **55**, 1050 (1997).
[20] M.E. Fisher, Phys. Rev. **176**, 257 (1968); M. Krech, in *Computer Simulation Studies in Condensed Matter Physics XII*, edited by D. P. Landau, S.P. Lewis, and H.B. Schuettler (Springer-Verlag, Heidelberg, 1999).